Electromagnetic Models of Co/Cross Polarization of Bicontinuous/DMRT in Radar Remote Sensing of Terrestrial Snow at X- and Ku-band for CoReH2O and SCLP Applications

Xiaolan Xu, *Student Member, IEEE*, Leung Tsang, *Fellow, IEEE*, and Simon Yueh, *Fellow, IEEE*

***Abstract*—In this paper, we study the scattering properties of the terrestrial dry snow by modeling the snow structure as Bi-continuous media. The model is applied to study the snow scattering characteristics at X-band and Ku-band that are two frequencies in the proposed Cold Regions Hydrology High-resolution Observatory (CoReH2O) mission by ESA and the proposed Snow and Cold Land Process (SCLP) mission by NASA. There are two variables in the Bi-continuous media that can be adjusted to generate various snow microstructures. The different snow structures are illustrated. The extinction properties and phase matrices are studied through the Monte Carlo simulations. For each realization, the Maxwell Equations are solved numerically to take into account the coherent wave interactions among the inhomogeneties. We demonstrated the frequency dependences of scattering coefficients, which can vary depending on the setup parameters of the bicontinuous media. The power law are compared with experiment data of extinction coefficients of terrestrial snow. The calculated extinction and phase matrices are combined in the Dense Media Radiative Transfer theory (DMRT). We obtain the 1st order solution by using the iterative method. The surface scattering from the snow–ground interface is included by searching the look up table of NMM3D. The results of co-polarization and cross polarization are compared with the POLSCAT Ku-band airborne data and X-band TerraSAR-X satellite data in North Slope, Alaska.**

***Index Terms*—Active remote sensing, bi-continuous media, CLPX II experiments, dense media, NMM3D, snow properties, surface scattering, volume scattering.**

I. Introduction

SNOW water equivalent is an essential element in the global water cycle. Melting snow provides an important source of the fresh water for many places in the world. The global mapping of the snow storage will advance the knowledge of the climate systems. Recently the satellite mission Cold Regions Hydrology High-resolution Observatory, (CoReH2O) [1], was proposed to ESA and the Snow and Cold Land Process (SCLP) Satellite Mission was recommended to NASA in the Decadal Study. Both of the missions are expected to overcome current deficit in snow observations and perform high-resolution, global snow mapping. The proposed synthetic aperture radar in CoReH2O mission operates at X (9.6 GHz) and Ku band (17.2 GHz) for both co- and cross-polarization [2]. The SCLP instruments are not decided, but are likely to have two polarizations and two frequencies in the similar range. It is known that the radar backscattering signals from the snow cover are sensitive to the snow structure (such as ice grain size, shape, aggregation status and wetness) as well as the underneath ground condition (frozen status, soil moisture, degree of roughness) [3], [4]. Therefore, to develop a strictly physical model can enrich the understanding of the relationship between the wave propagation and snow microstructures and provide physical insights to the future missions. In addition, the forward model can also be utilized to improve the retrieval algorithms of the snow properties [5]. In this paper, we focus on the snow scattering effect. In the model, we assume the snow cover areas are vegetation and forest free.

In the recent years, several ground experiments [6]–[8] were conducted to investigate the capability of active microwave sensors from C- to Ka-band to discriminate various natural snow cover situations. It indicates that the X-band and Ku-band would be an optimal configuration for monitoring the snow water equivalence change and estimating the parameters of the underlying ground surface. Recently, the airborne data was collected through CLPX II experiments [9]. The spaceborne QuikSCAT data is widely studied [10], [11]. These two experiments are using Ku-band instruments and both of datasets indicate strong correlation between the backscattering responses and the snow accumulation. Ground measurements were also conducted in Canada [12].

There are several empirical and theoretical methods existing in the literature. The most common way to model the snow is assumed the ice grains as spherical particles [13]. To calculate the scattering properties of the snow, the classical approach is to use the Mie scattering along with the independent addition [14]. However, the snow grains were packed densely. In order to account for the multiple scattering, the dense media radiative theory was derived [15], [16]. The other important aspect of the snow is the shape of the ice grains. J. Du and J.C. Shi [17] illustrate the effects of the non-spherical ice particles.

Manuscript received October 01, 2011; revised February 06, 2012; accepted March 03, 2012. Date of publication April 17, 2012; date of current version June 28, 2012. This work was supported in part by the National Aeronautics and Space Administration.

X. Xu and L. Tsang are with the Electrical Engineering Department, University of Washington, Seattle, WA 98195 USA (corresponding author, e-mail: xlxu@uw.edu).

S. Yueh is with the Jet Propulsion Laboratory, California Institute of Technology, Pasadena, CA 91109 USA.

Color versions of one or more of the figures in this paper are available online at http://ieeexplore.ieee.org.

Digital Object Identifier 10.1109/JSTARS.2012.2190719

In this paper, we restrict the snow scenario to be dry with no vegetation/forest covered and the air temperature is low enough that the ground is frozen. The frequency range is from X-band (9.6 GHz) to two Ku-band frequencies (13.4 GHz and 17.2 GHz). The layering effect (eg. Ice layer) can be taken into account by using multilayer DMRT [18]. However, in this paper, we concentrate on the snow microstructure. We will analyze both volume scattering and surface scattering at X band and two Ku bands for co polarization and cross polarization. The studies are important, since the relative contributions from surface and volume scattering should be clearly understood in both CoReH2O and SCLP missions. The frequency and polarization dependences of surface and volume scattering are elaborated in the following sections.

For volume scattering, we follow the approach of dense media radiative transfer theory. In DMRT, the extinction, absorption, and bistatic scattering phase matrix in the radiative transfer equations are calculated by taking into account the collective scattering effects. In the QCA/DMRT theory, the quasicrystalline approximation is used to calculate the phase matrix of densely packed sticky spheres. [19], [20]. In NMM3D/DMRT, the Foldy Lax multiple scattering equations are used to calculate the phase matrix for densely packed sticky spheres [16], [21]. In recent years, we proposed an alternative model of bicontinuous model to simulate the microstructures of snow [22]–[24]. The bi-continuous model is introduced to simulate the microstructures of the snow. This model is based on a continuous representation of interfaces between different phases or domains within the medium. The extinction coefficient, absorption coefficient and scattering phase matrix are calculated through the Numerical Maxwell Model of three-dimensional (NMM3D) simulations, which is based on the volume integral equation with the discrete dipole approximation (DDA). In solving the phase matrix, the scattered fields are decomposed into coherent and incoherent fields with the incoherent fields contributing to the scattering matrix. To reduce the number of required realizations, the 1–2 frame is used, which assumes the snow sample is statistical isotropic. The calculated results of phase matrices are substituted into the dense media radiative transfer equations, giving the biconinuous/DMRT theory.

In Section II, we described the computer generation of snow samples based on bicontinuous media and analyzed the important model parameters that relate to various microstructures. In Section III, we demonstrated the calculations of extinction coefficients and phase matrices using numerical solutions of Maxwell equations. In Section IV, the frequency dependences of extinctions were illustrated and compared with extinction measurements. In Section V, we fully characterized the radar responses from the snow scenario including volume scattering of the snow, which included the snow–ground interface interaction, and ground surface scattering. The simulated extinctions and phase matrices from Section V were applied into the Dense Media Radiative Equations to perform the snow volume scattering. The surface scattering was based on 3D full wave simulations of Numerical Maxwell Model in 3 Dimensional (NMM3D) rough surfaces [25]. In the simulation, direct search was performed through a pre-generated table calculated by

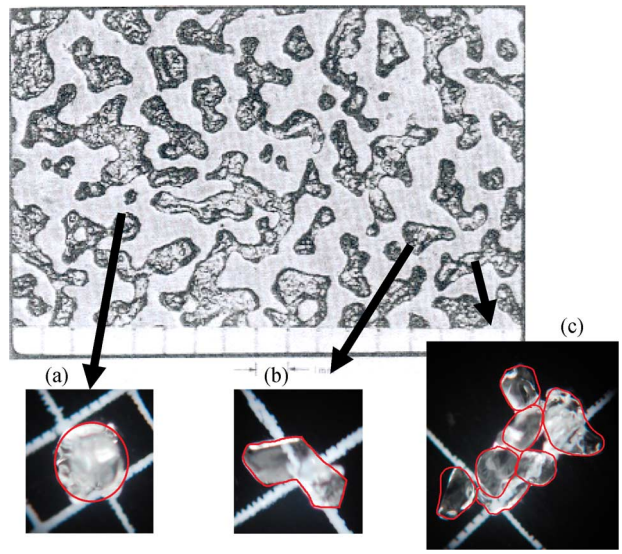

Fig. 1. Snow samples (a) Round shape (b) Facets (c) Melt-refreeze aggregate.

NMM3D. In Section VI, numerical results were illustrated for the combined volume scattering and surface scattering models in both X band and Ku band. In Section VII, Comparisons were made between the model results with Terra-SAR X band measurements and CLPX Ku band measurements. The conclusions were given in VIII.

II. Computer Generation of Snow Samples

To study the characteristic of snow, we need to establish the detailed snow structure. Dry snow is known a mixture of ice particles in the air background. The scattering signatures of the snow in the microwave frequency are highly dependent on the ice grain size, snow density, grain's shape and snow amount/depth. In the past, these particles were modeled as scatterers of definite shapes such as spheres or ellipsoids. Then, the snow sample was generated by randomly place the spheres or ellipsoids without overlapping each other. In real life, once the snow falls onto the ground, the metamorphism process starts. The form of the ice particles will be influenced by the temperature and pressure. The snow metamorphism existing in the snowpack can be divided into three types, equilibrium, kinetic and melt-freeze [26]. The equilibrium metamorphism tends to minimize the surface free energy of the ice particles by making them more round shape. (Fig. 1(a)) When the temperature gradients of the snowpack become large, the kinetic metamorphism will turn the ice particles into squares (Fig. 1(b)). The depth-hoar can be formed in this process. When the surface temperature becomes much warmer, the melt-freeze process dominates the formation of the ice grains. The ice grains melt in the daytime and refreeze at night causing a lot of larger and irregular shape (Fig. 1(c)). The random distributed sphere model can only describe the first type.

To represent the aggregated snow structure, the sticky spheres model is used [27]. In the sticky hard sphere model, the Percus-Yevick pair distribution function is introduced to account for the relative position of the spheres. The aggregates are formed by randomly bond two or three spheres. The stickiness parameter

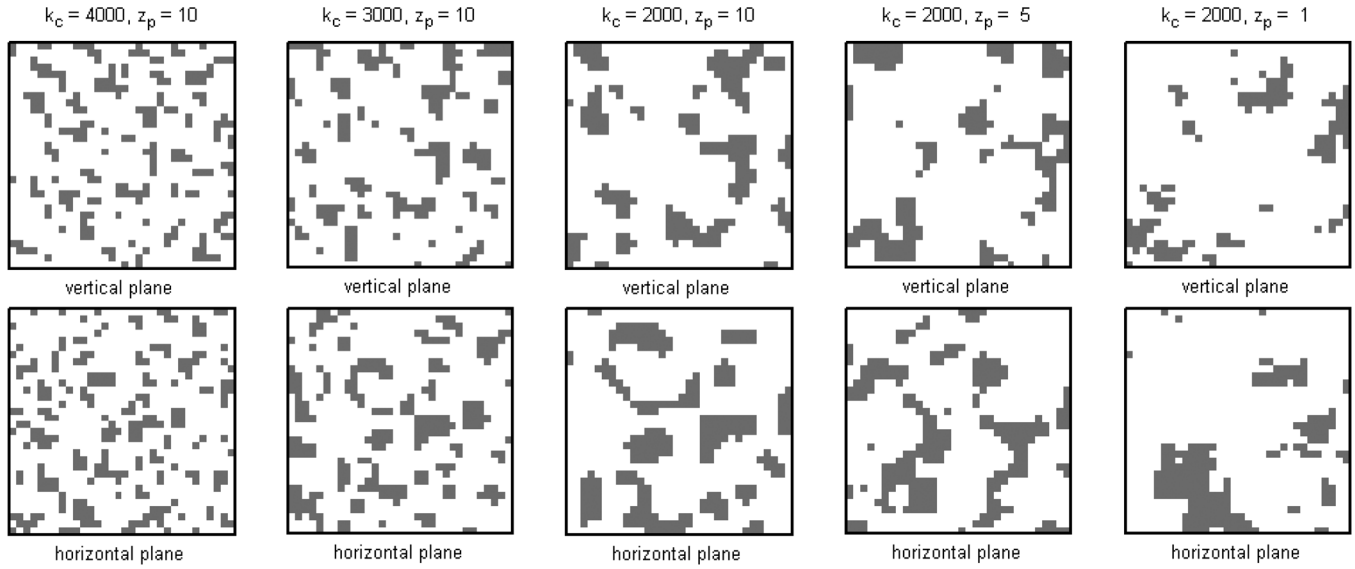

Fig. 2. The vertical and horizontal cross section of computer generated bi-continuous media with the different setup. The fractional volume is 20%.

is defined to measure the attraction between the particles. Based on the sticky spheres model, the generated snow microstructures are still limited. Recently, the bi-continuous media with discrete permittivities was used to describe snow sample of the irregular ice particle shape.

A. Bi-Continuous Model

The morphology of bi-continuous media is described by a function $S(\overline{r})$ in (1), which is a summation of N number of stochastic standing waves.

$$S(\overline{r}) = \frac{1}{\sqrt{N\langle A^2\rangle}} \sum_{n=1}^{N} A_n \cos(\overline{k}_n \cdot \overline{r} + \phi_n) \tag{1}$$

where $\langle A^2\rangle$ is the mean square amplitude. The random variables A_n, $\overline{k}_n$ and ϕ_n are independent with each other. In our model, the normalized amplitude is assumed as $A_n = 1$. ϕ_n is uniformly distributed on $[0, 2\pi)$ which means the media is statistically isotropic. The variable $\overline{k}_n$ is a spectral wave vector and its magnitude $|\overline{k}_n| = k$, with dimension inverse distance, represents the reciprocal of size. In this paper the units of k_c is 32 m^{-1}. The probability density function (2), of random variable k is assumed to obey Gamma distribution

$$p(k) = \frac{1}{\Gamma(z_p+1)} \frac{(z_p+1)^{z_p+1}}{k_c} \left(\frac{k}{k_c}\right)^{z_p} e^{-(z_p+1)\left(\frac{k}{k_c}\right)} \tag{2}$$

where k_c is the scale parameter, physically corresponding to the reciprocal of the average snow grain size and z_p is the shape parameter which controls the grain size distribution. Thus there are two parameters k_c and z_p that describes size. The parameter z_p is dimensionless and the parameter k_c has dimension inverse distance. In the previous sticky sphere model [20], there are also two parameters that describe size, namely the radius a and the sticky parameter τ.

The directions of the wave vector $\overline{k}_n$ are uniformly distributed over solid angle 4π. Based on central limit theorem, S(r) is Gaussian random process with $\langle \mathrm{S(r)}\rangle = 0$ and $\langle \mathrm{S^2(r)}\rangle = (1/2)$. Next the function Θ_α is an indicator function to level out the snow and ice cube, which is defined such that

$$\Theta_\alpha\left(S(\overline{r})\right) = \begin{cases} 1 & for\ S(\overline{r}) > \alpha \\ 0 & otherwise \end{cases} \tag{3}$$

α is the cutting levels specifying air and ice interfaces which can be determined by giving fractional volume [23].

For computer-generated structure, we choose a sample cubic of volume V that the side is usually larger than a wavelength to ensure the randomness. The sample cube is cut into subcells. Each subcell is filled with either ice or air depending on the fractional volume and random process function. In the following examples, we made superposition of 10^4 sinusoidal waves. To demonstrate different snow structure, we choose five cases by changing the setup (k_c, z_p) in Fig. 2. The fractional volume of the samples is fixed at 20%. The top plots show the vertical cross section and the bottom plots are the horizontal cross section. The plots of the first three columns are assigned the shape distribution parameter $z_p = 10$ and changing the scale parameter k_c. As the k_c increase, the scatters are gradually breaking into pieces. The last three columns keep $k_c = 2000$ constant and vary z_p. With the decreasing z_p, the scatters are tends to aggregate together. The bi-continuous model provides the flexibility of constructing complex snow microstructures. The asymmetric microstructures also effect the polarization of the scattering. Compared with Fig. 1, a larger k_c with a larger z_p can be used to model the fresh snow. For depth hoar, it can be modeled by decreasing k_c and z_p.

III. Extinction Coefficient and Phase Matrix

In this section, we will analyze the scattering characteristics of the snow sample in the microwave frequency. In the real snow condition, the density varies from 100 $\sim$ 400 kg/m3, which corresponding to fractional volume from 10% up to 45%. The collective scattering between the particles is significant, especially when the particles are bonded. To account the coherent wave interactions, analytically, the QCA is derived to calculate the extinction coefficient and phase matrix [28]. Distinct

from the classical Rayleigh-Mie scattering approach, the extinction coefficient calculated from QCA has lower frequency dependent and phase matrix has larger forward scattering [20]. In addition, the numerical method (NMM3D) is also performed using Foldy-Lax equations [21]. The Foldy-Lax is directly from the Maxwell's equation. The NMM3D results yield the similar properties as the QCA in the co-polarization phase matrix and simultaneously generated non-zero cross polarization in the phase matrix. The non-zero cross pol is mainly due to the near field interaction between the aggregated spheres in which the internal fields are not aligned. Fundamentally, the non-zero cross pol are a consequence of the asymmetric structure inherent in the aggregated sphere.

Now, we will examine the extinction coefficient properties and phase matrix of the Bi-continuous media. The incident wave is in the $\overline{k}_i$ direction and has electric field $\overline{E}_{inc}$ in the $\hat{e}_i$ direction that is perpendicular to the $\overline{k}_i$ plane wave

$$\overline{E}_{inc} = \hat{e}_i \exp(i\overline{k}_i \cdot \overline{r}). \tag{4}$$

When the bi-continuous structure was generated, the subcell was formed periodically. $\overline{r}$ is the center position of each subcell. Each subcell is randomly assigned as ice cube with relative permittivity of 3.2 and air cube with relative permittivity of 1. Here we assume the ice cube is concrete and the loss fact of the ice in X and Ku band is small and can be ignored. In the snow scale, we chose the subcell as 0.5 mm. The convergence of the discretization was demonstrated in [25]. The excitation field $\overline{E}(\overline{r})$ in each subcell is governed by the volume integral equation

$$\overline{E}(\overline{r}) = \overline{E}_{inc}(\overline{r}) + \omega^2\mu \int\limits_{\Delta V} d\overline{r}' \overline{\overline{G}}(\overline{r}, \overline{r}') [\varepsilon(\overline{r}) - \varepsilon_0] E(\overline{r}') \tag{5}$$

where ω is the angular frequency and μ is the permeability. The integration is over the whole snow sample. $\overline{\overline{G}}(\overline{r}, \overline{r}')$ is the dyadic green's function. $\varepsilon(\overline{r})$ is the permittivity of the subcell. Depending on the position $\overline{r}$, $\varepsilon(\overline{r})$ is either $3.2\varepsilon_0$ or ε_0. Similarly, the scattering wave $\overline{E}_s(\overline{r})$ can be also expressed in terms of $\overline{E}(\overline{r})$

$$\overline{E}_s(\overline{r}) = \omega^2\mu \left[\overline{\overline{I}} + \frac{\nabla\nabla}{k^2}\right] \int\limits_V d\overline{r}' \frac{\exp\left(i\overline{k} \cdot |\overline{r} - \overline{r}'|\right)}{|\overline{r} - \overline{r}'|} \varepsilon_f(\overline{r}') E(\overline{r}') \tag{6}$$

In the X and Ku-band, the subcell dimension is much smaller than the wavelength so that discrete dipole approximation can be used to solve the wave interaction in sample region. Let the dipole moment of the i th cube be p_i, we could rewrite (5) in the dipole form,

$$p_i = \alpha_i \overline{E}_{inc} - \alpha_i \sum_{j=1, j\neq i}^{N} -\frac{k^2}{\varepsilon} \overline{\overline{G}}(\overline{r}, \overline{r}') \cdot \overline{p}_j \tag{7}$$

For the ice cube, the polarizability α is

$$\alpha_i = \frac{\alpha_{ic}}{1 - \frac{\alpha_{ic}}{4\pi\varepsilon_0 v_0}\left[\left(\frac{4\pi}{3}\right)^{\frac{1}{3}}(kd)^2 + i\frac{2}{3}(kd)^3\right]}$$

$$\alpha_{ic} = 3\varepsilon v_0 \frac{\varepsilon_p - \varepsilon_0}{\varepsilon_p + 2\varepsilon_0}, \quad \varepsilon_p = 3.2\varepsilon_0 \tag{8}$$

v_0 is the volume of the subcell, and d is the subcell dimension.

For subcell occupied by air, $\alpha_i = 0$. The matrix equation is solved by using the generalized minimal residual method. The tolerance of the residual is set at 0.001. Both outer and inner iterations converge with 10 times. Since the subcells are periodic in spacing, the matrix vector multiplications are accelerated by FFT method. After getting each dipole moment for subcell, the far field scattering for one realization can be obtained

$$\overline{E}_s(\overline{r}) = \frac{k^2}{\varepsilon} \frac{\exp(ikr)}{4\pi r} (\hat{1}_s\hat{1}_s + \hat{2}_s\hat{2}_s) \cdot \sum_{j=1}^{N} \exp(-\overline{k}_s \cdot \overline{r}_j) \cdot \overline{p}_j \tag{9}$$

The scattering field is expressed in the 1–2 frame, where $\hat{1}_s, \hat{2}_s$ is unit vector, indicating the polarization. The 1–2 frame definition can be found in [16], [21], [23]. In random scattering problems, the fields and intensity are fluctuating as the sample structure has inhomogeneities that are randomly distributed. Unlike the deterministic problem in which there is only one solution, the random media problem only has a unique solution for a single realization. To describe the random process, the Monte Carlo simulation is performed. In this paper, we perform 60 realizations to ensure the convergence with realizations. The total scattered fields are decomposed in to coherent and incoherent field. Only the incoherent waves contribute into the scattering coefficient and phase matrix.

A. Coherent Field and Incoherent Field

The coherent wave can be obtained by averaging over realizations

$$\langle E_s(\theta_s, \phi_s)\rangle = \frac{1}{N_r} \sum_{\sigma=1}^{N_r} \overline{E}_s^{\sigma}(\theta_s, \phi_s) \tag{10}$$

where σ is the realization index, N_r denotes the number of realization. The incoherent field can be obtain by subtract the coherent field from the total scattering field.

$$\tilde{E}_s^{\sigma}(\theta_s, \phi_s) = \overline{E}_s^{\sigma}(\theta_s, \phi_s) - \langle E_s(\theta_s, \phi_s)\rangle \tag{11}$$

B. Phase Matrix and Extinction Coefficient

The extinction coefficient can be calculated by

$$\kappa_e = \kappa_a + \kappa_s \tag{12}$$

where κ_a is absorption coefficient. The absorption coefficient is calculated from the internal electric fields of the particles. The scattering coefficient κ_s is calculated by the integration of the phase matrix elements in the 1–2 frame as follows

$$\kappa_s = \pi \int\limits_0^{\pi} d\Theta \left(P_{11}(\Theta) + P_{22}(\Theta) + P_{12}(\Theta) + P_{21}(\Theta)\right) \sin(\Theta) \tag{13}$$

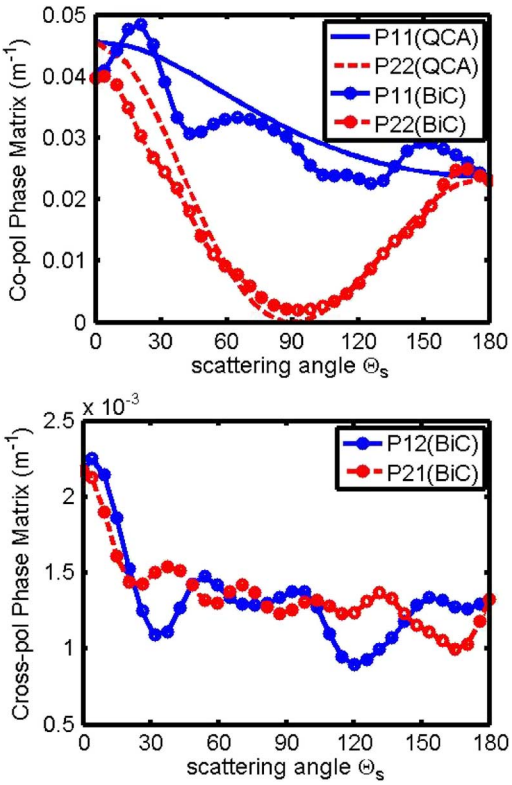

Fig. 3. The top one is the co-pol phase matrix comparison between QCA and numerical simulation of bicontinuous media in Ku-band (18.7 GHz). The setup for QCA: diameter $= 0.45$ mm fv $= 20\%$ tau $= 0.1$ The setup for bicontinuous media is $k_c = 3000$, $z_p = 10$ fv $= 20\%$.

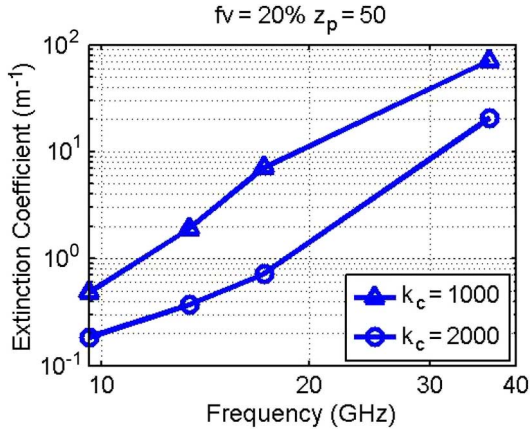

Fig. 4. The frequency dependence of extinction coefficient for the different k_c.

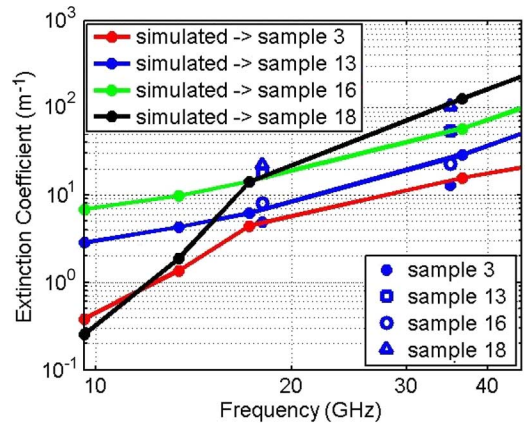

Fig. 5. Extinction coefficient comparison between the simulations and the measurements from snow sample.

Phase Matrix is defined as the bistatic scattering cross sections per unit volume.

$$\begin{bmatrix} \langle |E_{1s}|^2 \rangle \\ \langle |E_{2s}|^2 \rangle \end{bmatrix} = \begin{bmatrix} P_{11} & P_{12} \\ P_{21} & P_{22} \end{bmatrix} \begin{bmatrix} |\overline{E}_{1i}|^2 \\ |\overline{E}_{2i}|^2 \end{bmatrix} \tag{14}$$

In Fig. 3, the phase matrixes of co-polarization and cross polarization are illustrated. The co-polarization phase matrix has similar properties to the analytical QCA solution. The results also exhibit larger forward scattering. As mentioned in the previous section, the k_c corresponds to the reciprocal of the effective physical grain size. Therefore by choosing corresponding parameters between QCA and bicontinuous model, the scattering results from QCA and bicontinuous have similar scattering coefficients. The scattering coefficient from the QCA is 0.272 /m and from bicontinuous media is 0.269 /m. The bottom plot in Fig. 3 shows the cross-polarization phase matrix. The cross pol in the backscattering direction is only 18 times (12.5 dB) less than the co-pol in the case of fractional volume of 20%. The larger cross-polarization is due to the irregular shape of the generated ice particles in the bicontinuous media.

IV. Frequency Dependence of Extinction and Comparison with Extinctions Experiments

The frequency dependence of the extinction is studied for various parameters of k_c and z_p. In Fig. 4, we plot the extinction coefficient by increasing k_c. As the k_c increases, the effective grain size decreases, which lead to a smaller extinction coefficient. The frequency dependent index for the smaller grain size is around 4, while the other case shows lower frequency dependence, especially from X-band to Ku-band.

Next, we compared the extinction coefficient with the experiment data of extinction. The experiment was conducted at Radio Laboratory, Helsinki University of Technology in 1987. Here we examine four cases from Table II in [29]. Sample 13 and 16 are from the bottom layer of the snow with different snow density. The fractional volume used for these two samples are 30% and 40%. Sample 3 and 18 are the snow from the top layer with density of 217 kg/m3 and 351 kg/m3. In the simulations, we used the fractional volume of 20% and 30%. The sample 3 is fresh snow. In Fig. 5, we show the extinction coefficient from the simulations compare well with the experiment data. The bicontinuous setups for those four examples are listed in Table I.

V. DMRT and Backscattering Coefficients

In this section, we substitute extinction and phase matrix from the numerical results of bicontinuous media into the dense media radiative transfer (DMRT) equation. The DMRT equation is

$$\frac{d\overline{I}(\overline{r},\hat{s})}{ds} = -\kappa_e I(\overline{r},\hat{s}) + \int_{4\pi} d\Omega' \, \overline{\overline{P}}\,(\overline{r},\hat{s},\hat{s}') \cdot \overline{I}(\overline{r},\hat{s}) \tag{15}$$

TABLE I
BICONTIUOUS MEDIA SETUP FOR DATA COMPARISON

Sample Number	Scale Parameter k_c	Distribution shape Parameter z_p	Fractional Volume fv(%)
Sample 3	1500	10	20%
Sample 13	1000	10	30%
Sample 16	1500	10	40%
Sample 18	1000	50	30%

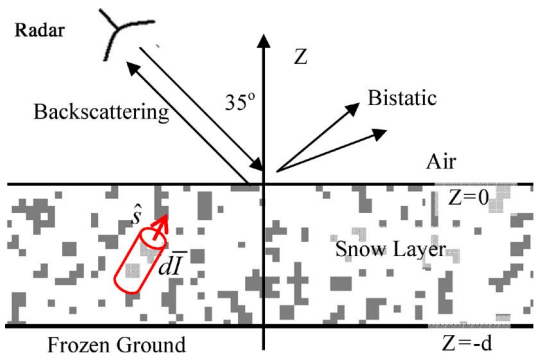

Fig. 6. Backscattering and bistatic scattering of terrestrial snow.

where $I(\overline{r}, \hat{s})$ is the specific intensity at $\overline{r}$ in direction $\hat{s}$, κ_e is extinction coefficient and $\overline{\overline{P}}$ is the phase matrix in the principal frame. Previously, we use the 1–2 frame to represent the phase matrix. Here we need to transform the phase matrix from the 1–2 frame to the principal frame through transformation matrix [20].

In the active remote sensing, we treat the snow as a random media layer above the frozen ground (Fig. 6). The boundary condition for the snow–air interface and snow–ground interface is

$$\overline{I}(\pi-\theta,\varphi,z=0) = r(\theta)\overline{I}(\theta,\varphi,z=0) + t(\theta_0)\overline{I}_0\delta(\cos\theta_0-\cos\theta_{0inc})\delta(\varphi-\varphi_{inc}) \quad (16)$$

$$\overline{I}(\theta,\varphi,z=-d) = r(\theta)\overline{I}(\pi-\theta,\varphi,z=-d) \quad (17)$$

We used iterative method to solve the DMRT equations. The iterative method assumes that the phase matrix is a small parameter. First order solution is solved and used in the following plots. In the first order scattering solution, there are four terms, which directly related to the phase matrix in the forward and backward direction. The explicit analytical solutions can be found in [20]. For illustration, the incident angles in Section V and Section VI are fixed at 35 degrees. In Figs. 7 and 8, we illustrate the bistatic scattering coefficient for Ku-band an X-band at $\mathrm{depth} = 0.3$ m, $k_c = 1500$, $z_p = 50$. In the past, for the sphere model, the first order RT solution only has co-polarization. In the bi-continuous model, the asymmetric structures lead to cross-polarization in the results. Moreover, the phase matrices are calculated though numerical simulation that include all the interactions between the subcells. In the

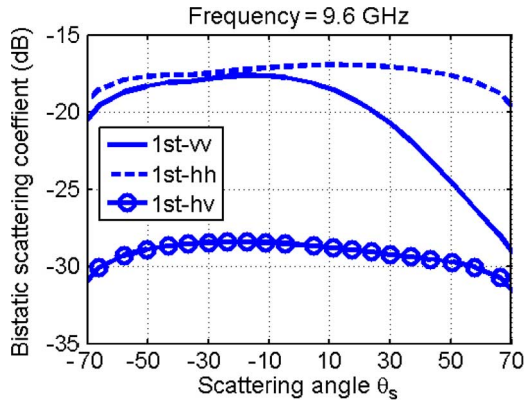

Fig. 7. Bistatic solution of the first order solution for co-pol and cross-pol at X-band (9.6 GHz).

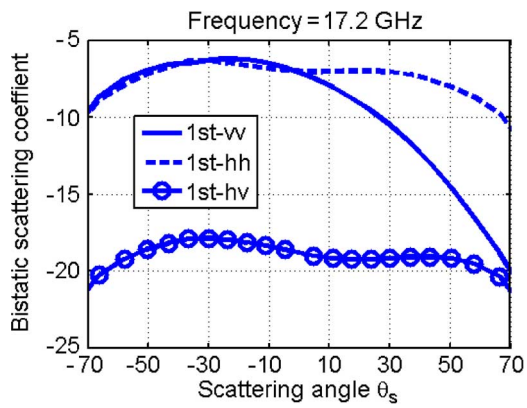

Fig. 8. Bistatic solution of the first order solution for co-pol and cross-pol at Ku-band (17.2 GHz).

backscattering direction (-35 degrees in Figs. 7 and 8), the cross-pol coefficients are only 10 dB lower than the co-pol.

In Fig. 9, we plot the backscattering coefficient as a function of snow depth. The co-polarization vv and cross polarization hv are illustrated for 9.6 GHz and 13.4 GHz, which are the operation frequency of TerraSAR and POLSCAT. The sensitivity of the backscattering coefficients to the snow depth is around the same in these two frequencies. In Fig. 10, we keep the same X-band but increase the Ku-band to 17.2 GHz, which are the two proposed frequency in the CoReH2O mission, and SCLP. In 17 GHz, the backscattering coefficients that are calculated from first order theory start to saturate when snow depth is beyond 60 cm.

VI. NUMERICAL RESULTS AND DISCUSSIONS

In this section, we include the rough surface scattering of the underlying ground and discuss the total scattering due to the terrestrial snow.

For surface scattering, in the past, analytic methods such as Kirchhoff method (KA), small perturbation method (SPM) and advanced integral equation model (AIEM) [30] have been used to analyze scattering by random rough surfaces. In this paper, the surface scattering is calculated through the numerical method of large-scale 3D random rough surfaces. The simulation is based on the Method of Moment and accelerated by the Sparse Matrix Canonical Grid (SMCG) method the Physical

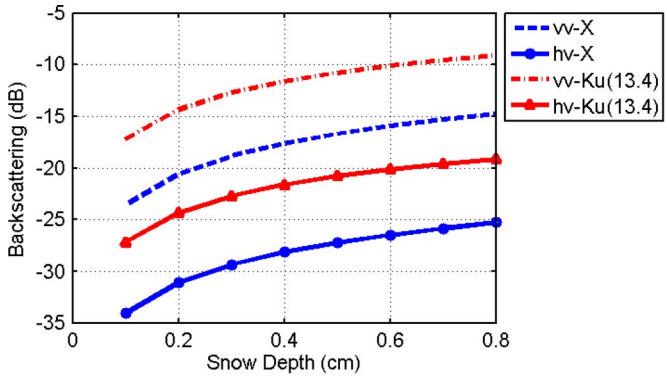

Fig. 9. Backscattering coefficient as a function of snow depth at 9.6 GHz (X-band) and 13.4 GHz (Ku-band).

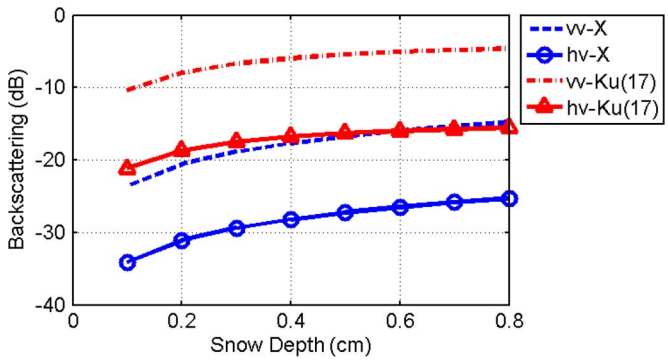

Fig. 10. Backscattering coefficient as a function of snow depth at 9.6 GHz (X-band) and 17.2 GHz (Ku-band).

Based Two Grid (PBTG) method [31]. Hundreds of cases were computed and look-up tables were created.

There are two advantages of using the NMM3D. First of all, it can handle larger rms height than traditional small perturbation method. Secondly, both co-polarization and cross-polarization can be computed. The total scattering is

$$\sigma_t = \sigma_{DMRT}(kc, zp, fv, d, r_p) + \sigma_{surface} \exp(-2\kappa_e d/\cos\theta_i) \tag{18}$$

where σ_{DMRT} is the backscattering calculated from the in-DMRT model. It related to the structure of the bicontinuous media (k_c, z_p, f_v) and the snow depth d. The $r_p(p : v/h)$ is the coherent reflectivity from the rough surface look up table. $\sigma_{surface}$ is the rough surface scattering from the look up table. In Fig. 11, we plot total backscattering of three frequencies as well as the volume scattering from the snow layer and ground rough surface layer. The ground surface is assumed to be frozen with permittivity of $3.5 + 0.001$i and rms height of 3 mm, correlation length of 12 mm. In the X-band, the surface scattering is comparable to the snow volume scattering. The total backscattering sensitivity to the snow depth becomes weak. As the frequency increase, both surface scattering and volume scattering part are increased. However, the volume scattering grows faster. Therefore, at 17.2 GHz, the total scattering is dominated by the snow volume scattering.

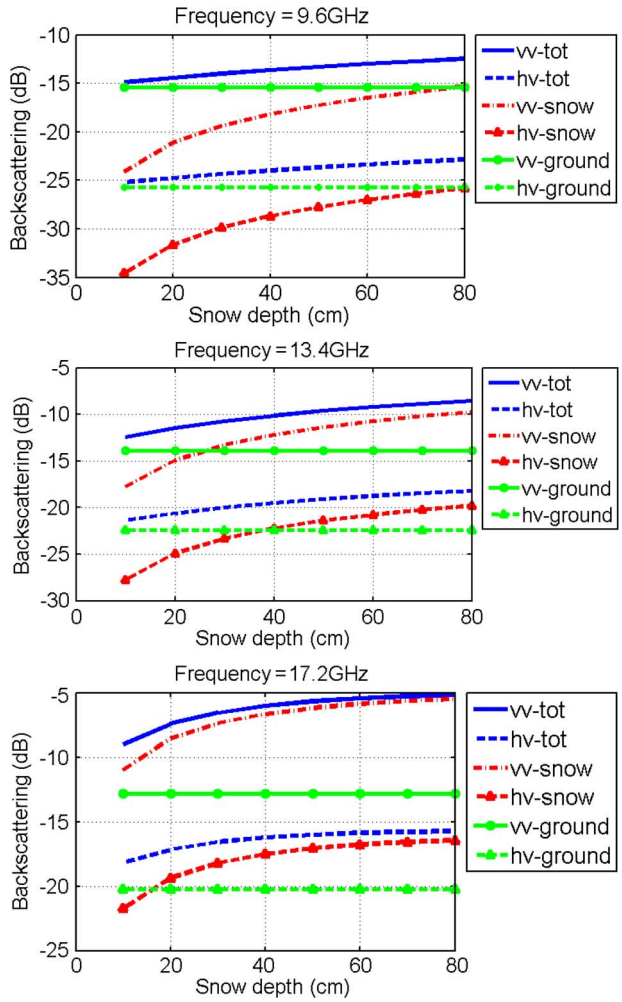

Fig. 11. The total backscattering, decomposed snow scattering and ground scattering for X-band and two Ku-band frequency with fv $= 20\%$, $k_c = 15000$, $z_p = 50$.

VII. Comparison with Field Experiments

To farther validate the bicontinuous DMRT model, we compare the simulation data with the experiment data. The datasets includes measurements from two frequencies. The Ku-band data were collected by JPL POLSCAT radar as part of the second Cold Land Processes Field Experiment (CLPX II).

POLSCAT is a Ku-band polarimetric scatterometer operating at 13.4 GHz with 100 m footprints. It can record four channel (VV, HH, VH, HV) radar responses simultaneously. The POLSCAT radar was installed on a Twin Otter aircraft and operated at a 35-degree. In winter from 2006–2008, over twenty flights were flown over the Rocky Mountains in Colorado and the North Slope of Alaska. The data used in this paper is from Feb 18 $\sim$ 24, 2008 at the Kuparuk River. The X-band datasets was collected simultaneously through the German Aerospace Center (DLR) spaceborne TerraSAR-X Synthetic Aperture Radar. The resolution of the TerraSAR-X is 10 m and the average incident angle at 45 degree. The snowpit was sampled at the same time. The relative position for the ground snowpit area and two radars response coverage was indicated in Fig. 12.

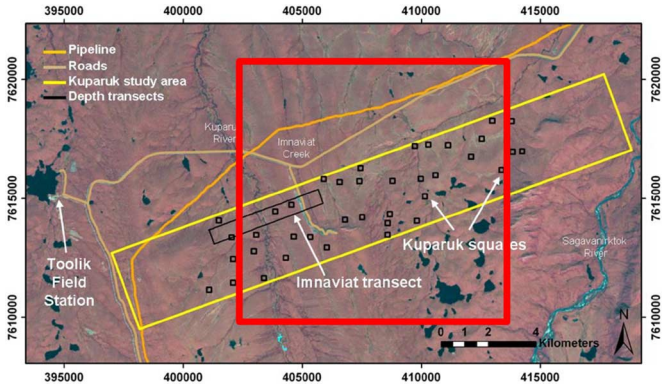

Fig. 12. X-band (red box) and Ku band (Yellow box) data coverage. The snowpit samples locations are the black squares.

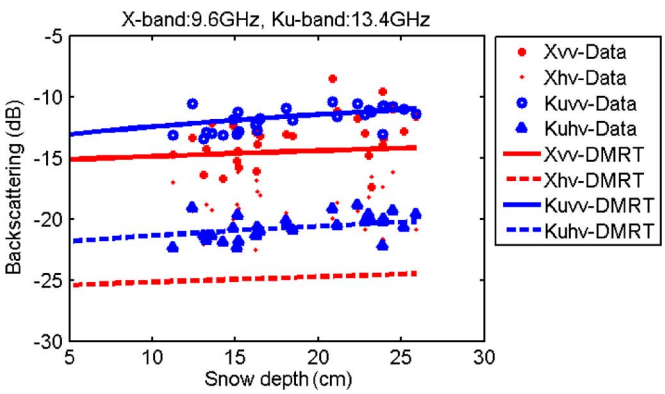

Fig. 13. Comparison between the measurement data from Ku-band and X-band and the DMRT simulation.

In Fig. 13, we show the comparison between the model results and measurement data. The bicontinuous setup for the simulation is $k_c = 1500$, $z_p = 50$ for all the snowpit shown in Fig. 12. The setup is according to the snow pit record in CLPX II, where larger grain size structure (such as depth hoar) has been reported. The fractional volume in the simulation is fixed at 20%. It's not explicit to apply the snow measurement directly from the field such as snow grain size. The setup in the simulation is a best fit parameter. In the Ku-band, the DMRT simulation could match both co-polarization and Cross-polarization. However, in the X-band, due to the fine resolution, the backscattering data has larger fluctuation. For the co-polarization, the simulation could catch increasing change and give relative same absolute value, while the cross-pol backscattering simulation shows much lower than the measurement data. That is due to the noise level of the TerraSAR-X is around 20 dB which make the measurement below 20 dB not reliable.

VIII. Conclusion

In this paper, we introduce bi-continuous random media morphology to generate snow sample cubic. By controlling the distribution of the wavenumber, the bi-continuous random media model can describe more complicated snow condition. The scattering properties are studied by numerically solving the Maxwell's Equations exactly. The extinction coefficient and phase matrix then were combined with DMRT equations to calculate the volume scattering from the snow layer. The rough surface ground backscattering effects are included. We demonstrate the rough surface influence over X-band to Ku-band. Finally, we validate the bicontinuous DMRT with the experiments data. The physical models in this paper are based on numerical solutions of Maxwell equations for both volume scattering and surface scattering. In implementation for satellite missions, the simulated results of Maxwell equations are used to prepare look-up tables so that retrievals algorithms can be operated in real time.

References

[1] H. Rott, D. Cline, C. Duguay, R. Essery, C. Haas, G. Macelloni, E. Maines, J. Pulliainen, H. Rebhan, and S. Yueh, "CoReH2O—A Ku- and X-band SAR mission for snow and ice monitoring," in *Proc. Eur. Conf. Synthetic Aperture Radar*, Friedrichshafen, Germany, 2008.

[2] H. Rott, S. Yueh, D. W. Cline, C. Duguay, R. Essery, C. Haas, F. Hélière, M. Kern, G. Macelloni, E. Malnes, T. Nagler, J. Pulliainen, H. Rebhan, and A. Thompson, "Cold regions hydrology high-resolution observatory for snow and cold land processes," *Proc. IEEE*, vol. 98, pp. 752–765, May 2010.

[3] L. Tsang, J. A. Kong, and K. H. Ding, *Scattering of Electromagnetic Waves vol. 1. Theory and Applications*. Hoboken, NJ: Wiley-Interscience, 2000, ch. 4.

[4] C. Mätzler, "Applications of the interaction of microwaves with the natural snow cover," *Remote Sens. Rev.*, vol. 2, p. 287, 1987.

[5] J. Shi and J. Dozier, "Estimation of snow water equivalence using SIR-C/X-SAR. I. Inferring snow density and subsurface properties," *IEEE Trans. Geosci. Remote Sens.*, vol. 38, no. 6, pp. 2465–2474, Nov. 2000.

[6] T. Strozzi and C. Mätzler, "Backscattering measurements of Alpine snow-covers at 5.3 and 35 GHz," *IEEE Trans. Geosci. Remote Sens.*, vol. 36, no. 3, pp. 838–848, May 1998.

[7] M. Brogioni, G. Macelloni, G. , S. Paloscia, P. Pampaloni, S. Pettinato, and E. Santi, "Monitoring snow cover characteristics with multifrequency active and passive microwave sensors," in *Proc. IGARSS 2006*, Jul. 2006, pp. 2167–2170.

[8] K. Morrison, H. Rott, T. Nagler, H. Rebhan, and P. Wursteisen, "The SARALPS-2007 measurement campaign on X and Ku-Band Backscatter of snow," *Proc. IGARSS 2007*, pp. 1207–1210, July 23–28, 2007.

[9] D. Cline, K. Elder, S. Yu eh, J. Entin, H. Rott, and T. Nagler, "Overview of the second cold land processes experiment (CLPX-II)," in *Proc. IGARSS 2007*, Barcelona, Spain, 2007.

[10] S. V. Nghiem and W.-Y. Tsai, "Global snow cover monitoring with spaceborne Ku-band scatterometer," *IEEE Trans. Geosci. Remote Sens.*, vol. 39, no. 10, pp. 2118–2134, Oct. 2001.

[11] S. Yueh, S. Dinardo, A. Akgiray, R. West, D. Cline, and K. Elder, "Airborne Ku-band polarimetric radar remote sensing of terrestrial snow cover," *IEEE Trans. Geosci. Remote Sens.*, vol. 47, no. 10, pp. 3347–3364, 2009.

[12] R. Kelly, C. Duguay, J. King, G. Gunn, A. Kasurak, C. Derksen, P. Toose, A. Silis, A. Langlois, A. Royer, and N. Rutter, "The Canadian CoReH2O Snow and Ice (CAN-CSI) experiment 2009–2011," in *Proc. IGARSS 2011*, Vancouver, Canada, Jul. 2011.

[13] L. Tsang, J. A. Kong, and R. Shin, *Theory of Microwave Remote Sensing*. New York: Wiley, 1985, ch. 6.

[14] A. Wiesmann, C. Fierz, and C. Mätzler, "Simulation of microwave emission from physically modeled snowpacks," *Annals of Glaciology*, vol. 31, no. 1, pp. 397–405(9), Jan. 2000.

[15] L. Tsang and J. A. Kong, *Scattering of Electromagnetic Waves, vol. 3, Advanced Topics*. Hoboken, NJ: Wiley Interscience, 2001, ch. 6.

[16] X. Xu, D. Liang, L. Tsang, K. M. Andreadis, E. G. Josberger, D. P. Lettenmaier, D. W. Cline, and S. Yueh, "Active remote sensing of snow using NMM3D/DMRT and comparison with CLPX II airborne data," *IEEE J. Sel. Topics Appl. Earth Observ. Remote Sens.*, vol. 3, pp. 689–697, 2010.

[17] J. Y. Du, J. C. Shi, and H. Rott, "Comparison between a multi-scattering and multi-layer snow scattering model and its parameterized snow backscattering model," *Remote Sens. Environ.*, vol. 114, pp. 1089–1098, 2010.

[18] D. Liang, X. Xu, L. Tsang, K. M. Andreadis, and E. G. Josberger, "Multi-layer effects in passive microwave remote sensing of dry snow using dense media radiative transfer theory (DMRT) based on quasicrystalline," *IEEE Trans. Geosci. Remote Sens.*, vol. 46, no. 11, pp. 3663–3671, Nov. 2008.
[19] L. Tsang, C. T. Chen, A. T. C. Chang, J. Guo, and K. H. Ding, "Dense media radiative transfer theory based on quasicrystalline approximation with application to passive microwave remote sensing of snow," *Radio Sci.*, vol. 35, no. 3, pp. 731–749, May–Jun. 2000.
[20] L. Tsang, J. Pan, D. Liang, Z. X. Li, D. Cline, and Y. H. Tan, "Modeling active microwave remote sensing of snow using dense media radiative transfer (DMRT) theory with multiple scattering effects," *IEEE Trans. Geosci. Remote Sens.*, vol. 45, pp. 990–1004, 2007.
[21] K. K. Tse, L. Tsang, C. H. Chan, K. H. Ding, and K. W. Leung, "Multiple scattering of waves by dense random distribution of sticky particles for applications in microwave scattering by terrestrial snow," *Radio Science*, vol. 42, Sept. 2007.
[22] X. Xu, K. H. Ding, and L. Tsang, "Microwave scattering properties of dry snow using the bi-continuous random media," in *Proc. IGARSS 2009*, Jul. 2009.
[23] K. H. Ding, X. Xu, and L. Tsang, "Electromagnetic scattering by bicontinuous random microstructures with discrete permittivities," *IEEE Trans. Geosci. Remote Sens.*, vol. 48, no. 8, pp. 3139–3151, 2010.
[24] X. Xu, L. Tsang, and S. Yueh, "Electromagnetic models of like-polarization and cross-polarization in radar remote sensing of terrestrial snow at X- and Ku-band for CoReH2O and SCLP application," in *Proc. IGARSS 2011*, Jul. 2011.
[25] S. Huang, L. Tsang, E. G. Njoku, and K. S. Chen, "Backscattering coefficients, coherent reflectivities, and emissivities of randomly rough soil surfaces at L-band for SMAP applications based on numerical solutions of Maxwell equations in three-dimensional simulations," *IEEE Trans. Geosci. Remote Sens.*, vol. 48, no. 6, pp. 2557–2568, Jun. 2010.
[26] H. Bader, "Snow and its metamorphism," Snow, Ice and Permafrost Research Establishment, U.S. Army Corps of Engineers, 1954.
[27] K. H. Ding, L. Tsang, and S. E. Shih, "Monte Carlo simulation of particle positions for densely packed multi-species sticky particles," *Microw. Opt. Technol. Lett.*, vol. 30, pp. 187–192, 2001.
[28] C. T. Chen, L. Tsang, J. Guo, A. T. C. Chang, and K. H. Ding, "Frequency dependence of scattering and extinction of dense media based on three-dimensional simulations of Maxwell's equations with applications to snow," *IEEE Trans. Geosci. Remote Sens.*, vol. 41, no. 8, pp. 1844–1852, Aug. 2003.
[29] Hallikainen, M. F. Ulaby, and T. Deventer, "Extinction behavior of dry snow in the 18- to 90-GHz rage," *IEEE Trans. Geosci. Remote Sens.*, vol. GRSS-25, pp. 737–745, 1987.
[30] K. S. Chen, T. D. Wu, L. Tsang, Q. Li, J. C. Shi, and A. K. Fung, "Emission of rough surfaces calculated by the integral equation method with comparison to three-dimensional moment method simulations," *IEEE Trans. Geosci. Remote Sens.*, vol. 41, no. 1, pp. 99–101, 2003.
[31] P. Xu and L. Tsang, "Scattering by rough surface using a hybrid technique combining the multilevel UV method with the sparse-matrix canonical grid method," *Radio Sci.*, vol. 40, p. RS4012, 2005.

Xiaolan Xu (S'09–M'12) received the B.Eng. degree from Zhejiang University, Hangzhou, China in 2006, and the M.S. and Ph.D. degrees in electrical engineering from the University of Washington, Seattle, in 2008 and 2012, respectively.

She is now a postdoctoral scholar, working with the Water and Carbon Cycles Group in Jet Propulsion Laboratory (JPL), California Institute of Technology, Pasadena. Her research interests include theoretical and numerical studies in random media and application in microwave remote sensing of environment.

Leung Tsang (S'73–M'75–SM'85–F'90) was born in Hong Kong. He received the S.B., S.M., and Ph.D. degrees from the Massachusetts Institute of Technology, Cambridge.

Presently, he is a Professor of the Department of Electrical Engineering at the University of Washington, Seattle, where he has taught since 1983. He was the Chair of the Department from 2006 to 2011. Between 2001 and 2004, while on leave from the University of Washington, he was a Professor Chair with the Department of Electronic Engineering at the City University of Hong Kong. He is the lead author of 4 books. (1) Theory of Microwave Remote Sensing (Wiley-Interscience, 1985) and Scattering of Electromagnetic Waves, Volumes 1,2 and 3 (2001). His current research interests are in remote sensing and geoscience applications, signal integrity in interconnects, and computational electromagnetics and optics.

Prof. Tsang was the Editor-in-Chief of the IEEE TRANSACTIONS ON GEOSCIENCE AND REMOTE SENSING. He received the IEEE Geoscience and Remote Sensing Society Outstanding Service Award in 2000 and the IEEE Third Millennium Medal in 2000. He received the Distinguished Achievement Award of the IEEE Geoscience and Remote Sensing Society in 2008 and the "Fiorino Oro" (Golden Florin) Prize, from CeTeM, Italy, 2010. He was a Fellow of the Optical Society of America from 1996 to 2001. He was the President of IEEE Geoscience and Remote Sensing Society for the two-year term 2006–2007. He has been on the Editorial Board of the PROCEEDINGS OF IEEE since 2007. He was the Chair of the IEEE Technical Activities Board (TAB) Periodicals Committee in 2008–2009 and the Chair of the IEEE TAB Periodicals Review and Advisory Committee in 2010–2011. Since April 2008, he has been the President of the Electromagnetics Academy.

Simon H. Yueh (M'92–SM'01–F'09) received the Ph.D. degree in electrical engineering from the Massachusetts Institute of Technology, Cambridge, in January 1991.

He was a Postdoctoral Research Associate at the Massachusetts Institute of Technology from February to August 1991. In September 1991, he joined the Radar Science and Engineering Section, Jet Propulsion Laboratory (JPL), California Institute of Technology, Pasadena. He was the Supervisor of the Radar System Engineering and Algorithm Development Group from 2002 to 2007. He became the Deputy Manager of the Climate, Oceans and Solid Earth section in July 2007 and was promoted to Section Manager in March 2009. He is also serving as the Instrument Scientist for the National Aeronautics and Space Administration (NASA) Aquarius mission for global sea surface salinity observations. He has been the Principal/Co-Investigator of numerous research projects, including the polarimetric wind radiometer research; airborne scatterometer project for hurricane wind measurements, Passive/Active L-band Sensor (PALS) project, NASA Instrument Incubator Project for a mission concept using a large mesh-deployable antenna for soil moisture and ocean salinity sensing, the airborne polarimetric radar (POLSCAT) for ocean wind velocity measurements, the POLSCAT/Cold Land Processes Experiments (CLPX-1 and -2) in 2002–2004 and 2006–2008, the Advanced Component Technology lightweight dual-frequency antenna feed project, the Aquarius PALS High Wind Campaign in 2009, the POLSCAT-CLPX3 experiment in 2009–2010. He is leading the development of the Snow and Cold Land Processes mission concept at JPL. He is the author of four book chapters and more than 150 publications and presentations.

Dr. Yueh is an Associate Editor for the IEEE TRANSACTIONS ON GEOSCIENCE AND REMOTE SENSING. He is the recipient of the 2002 IEEE Geoscience and Remote Sensing Society (GRSS) Transaction Prize Paper Award, the 2000 Best Paper Award in the IEEE International Geoscience and Remote Symposium 2000, and the 1995 IEEE GRSS Transaction Prize Paper Award for a paper on polarimetric radiometry. He received the JPL Lew Allen Award in 1998 and Ed Stone Award in 2003.